

ARTICLE OPEN



Emergence and control of complex behaviors in driven systems of interacting qubits with dissipation

A. V. Andreev¹, A. G. Balanov^{2,✉}, T. M. Fromhold³, M. T. Greenaway², A. E. Hramov¹, W. Li³, V. V. Makarov¹ and A. M. Zagoskin^{2,4,✉}

Progress in the creation of large-scale, artificial quantum coherent structures demands the investigation of their nonequilibrium dynamics when strong interactions, even between remote parts, are non-perturbative. Analysis of multiparticle quantum correlations in a large system in the presence of decoherence and external driving is especially topical. Still, the scaling behavior of dynamics and related emergent phenomena are not yet well understood. We investigate how the dynamics of a driven system of several quantum elements (e.g., qubits or Rydberg atoms) changes with increasing number of elements. Surprisingly, a two-element system exhibits chaotic behaviors. For larger system sizes, a highly stochastic, far from equilibrium, *hyperchaotic* regime emerges. Its complexity systematically scales with the size of the system, proportionally to the number of elements. Finally, we demonstrate that these chaotic dynamics can be efficiently controlled by a periodic driving field. The insights provided by our results indicate the possibility of a reduced description for the behavior of a large quantum system in terms of the transitions between its qualitatively different dynamical regimes. These transitions are controlled by a relatively small number of parameters, which may prove useful in the design, characterization, and control of large artificial quantum structures.

npj Quantum Information (2021)7:1 | <https://doi.org/10.1038/s41534-020-00339-1>

INTRODUCTION

Recent progress in experimental techniques for the fabrication, control and measurement of quantum coherent systems has allowed the routine creation of moderate-to-large arrays of controllable quantum units (e.g., superconducting qubits, trapped atoms and ions) expected to have revolutionary applications, e.g., in sensing, quantum communication and quantum computing^{1–4}. They also allow the investigation of fundamental physics, such as the measurement problem^{5–7}, the link between the chaotic behavior in classical systems and the corresponding dynamics in their quantum counterparts^{8–12} and the relative roles of entanglement and thermalization^{13–17}.

The deployment of modern quantum technologies generally requires both the improvement of unit quantum elements (e.g., increasing their decoherence times) and the scaling up of quantum structures¹⁸.

It is known that large systems comprising many functional elements tend to demonstrate emergent phenomena in their dynamics, which cannot be observed in smaller systems^{19,20}. Examples include dynamical phases in driven Bose–Einstein condensates²¹, synchronization in micromechanical oscillator arrays²², and coherent THz emission from layered high-temperature superconductors^{23–25}. Nevertheless, the emergent phenomena are commonly neglected when designing and investigating large-scale coherent structures. This is possibly due to the absence of a convenient theoretical framework for studying these novel systems. One important open question to be tackled is how the dynamics scales with the increase of the system size (e.g., number of qubits) and what role in its change is played by emergent phenomena.

We address these questions by studying theoretically the far-from-equilibrium dynamics of a driven chain of interacting

two-level quantum systems with dissipation and dephasing (Fig. 1a). We find that even a short chain comprising between two and four elements can demonstrate chaotic behavior. Remarkably, in systems with five or more elements a phenomenon known as hyperchaos emerges, a dynamical regime characterized by two or more positive Lyapunov exponents. Hyperchaos has features that resemble thermalization even though the system is far from equilibrium. We show that, in contrast to thermalization, the deterministic origin of hyperchaos allows it to be controlled either by tuning of the system parameters or by applying an external driving force. Our results give new insights into the dynamics of large artificial quantum coherent structures, which will be important for the design and control of quantum systems, such as Rydberg molecules, quantum information processors, simulators, and detectors.

RESULTS

Mathematical model

Here we investigate the dynamics of a one-dimensional (1D) chain of N qubits driven by an external electromagnetic field in the presence of decoherence. The system under consideration is equivalent to a system of Rydberg atoms, by rescaling and reidentification of parameters^{26–31}. Along with superconducting structures, Rydberg systems provide a controllable testbed for studying fundamental quantum dynamics^{32–34} and for developing new quantum chemistry^{35–37}. In particular, arrays of Rydberg atoms can be controlled experimentally with very high precision^{38–40}. Each atom has a ground state $|g\rangle$ and an electronically excited high-energy Rydberg state $|e\rangle$ (Fig. 1b). Rydberg states have large polarizability $\sim n^7$ (where n is the principal quantum

¹Innopolis University, Universitetskaya Str. 1, Innopolis 420500, Russia. ²Department of Physics, Loughborough University, Loughborough LE11 3TU, UK. ³School of Physics and Astronomy, University of Nottingham, Nottingham NG7 2RD, UK. ⁴Department of Theoretical Physics and Quantum Technologies, National University of Science and Technology MISIS, 4 Leninsky Avenue, Moscow 119049, Russia. ✉email: a.balanov@lboro.ac.uk; a.zagoskin@lboro.ac.uk

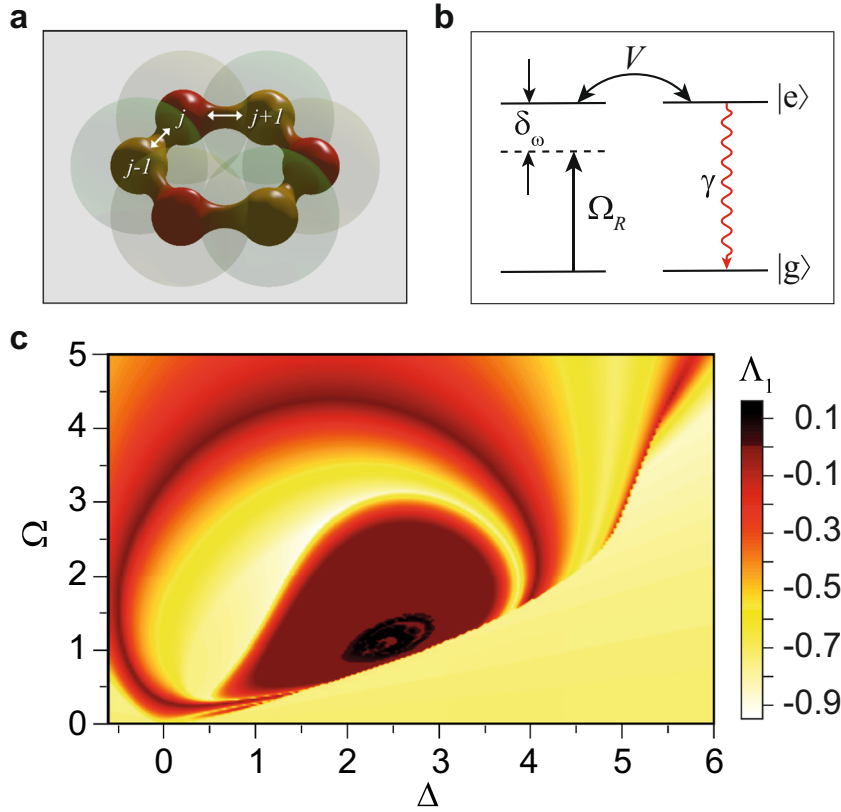


Fig. 1 Schematic representation of interacting qubits and the largest Lyapunov exponent dependence on model parameters for the case of two qubits. **a** Schematic representation of a circular chain of six interacting quantum units (e.g., Rydberg atoms or qubits), labeled by integer indexes and coupled via nearest neighbor interactions. **b** Atomic-level configuration reflected in the model [Eqs. (1)–(3)]. Coherent laser excitation from the ground state $|g\rangle$ to an excited (“Rydberg”) state $|e\rangle$ with a Rabi frequency Ω_R and detuning δ_ω , incoherent spontaneous decay γ , and the Rydberg interaction when an excited qubit shifts the transition frequency of a neighboring qubit by V . **c** Dependence of the largest Lyapunov exponent Λ_1 on Δ and Ω calculated for $c=5$ for the system of 2 coupled qubits. The color scale intensity indicates the value of Λ_1 .

number), which generates strong and long-range interactions between atoms⁴¹.

To model an electromagnetically driven array of qubits (Rydberg atoms), we use the Hamiltonian

$$H = \sum_{j=1}^N \left[-\delta_\omega |e\rangle\langle e|_j + \frac{\Omega_R}{2} (|e\rangle\langle g|_j + |g\rangle\langle e|_j) \right] + \sum_{j<k} V_{ij} |e\rangle\langle e|_j \otimes |e\rangle\langle e|_k, \quad (1)$$

where $\delta_\omega = \omega_l - \omega_0$ is the detuning between the laser and transition frequencies, Ω_R is the Rabi frequency (tuned by the laser field amplitude), and V_{ij} characterizes the interaction between i th and j th qubits.

The dynamics are described by the Liouville–von Neumann equation for the density matrix ρ ,

$$\dot{\rho} = -i[H, \rho] + \mathcal{L}[\rho], \quad (2)$$

where relaxation and dephasing processes are taken into account through the appropriate Lindblad operator

$$\mathcal{L}[\rho] = \gamma \sum_j \left[|g\rangle\langle e|_j \rho |e\rangle\langle g|_j - \frac{1}{2} \{ |e\rangle\langle e|_j, \rho \} \right], \quad (3)$$

with γ to be the decay rate from the excited state to the ground state. Rydberg atom interactions can range over a few tens of micrometers, larger than the physical size of the system (The same is true for superconducting qubits interacting through a resonator field mode.). Therefore, to simplify the analysis, we can initially assume that interactions are identical for any pair of qubits, $V_{ij} = V$

(see Fig. 1a, b). For a system of N qubits, ρ has the dimensionality of its Hilbert space, 2^N .

This problem can be greatly simplified by substituting a fully factorized density matrix approximation, $\rho \approx \prod_j \otimes \rho_j$, in Eq. (2). Here ρ_j is the (one-particle) density matrix of the j th qubit. This approximation is justified for a partially quantum coherent system, for which it has been shown accurately to describe experimental measurements on qubits, up to the corrections due to two-point correlations^{38,42–45}. In such a case, the quantum coherence between spatially separated elements is disrupted, e.g., by local ambient noise⁴⁶.

Rewriting the factorized density matrix ρ in terms of the population inversion of the j th qubit, $w_j = (\rho_j)_{11} - (\rho_j)_{00}$, and its coherence, $q_j = (\rho_j)_{10} = (\rho_j)_{01}^*$, yields:

$$\begin{aligned} \dot{w}_j &= -2\Omega \Im q_j - (w_j + 1); \\ \dot{q}_j &= i \left[\Delta - c \sum_{k \neq j} (w_k + 1) \right] q_j - \frac{1}{2} q_j + i \frac{\Omega}{2} w_j. \end{aligned} \quad (4)$$

In Eq. (4), the dimensionless time $\tau = \gamma t$ (i.e. $\dot{x} \equiv dx/d\tau = \gamma^{-1} dx/dt$), $\Omega = \Omega_R/\gamma$, $\Delta = \delta_\omega/\gamma$, and $c = Va/\gamma$, where a is the lattice constant. In more detail, the derivation of Eq. (4) is discussed in Section A in Supplementary Information.

Emergence of chaos and hyperchaos

Here we study the dynamical regimes of chains of interacting qubits. To characterize the complexity (randomness) of the emergent chaos and hyperchaos, we calculate the full spectrum of the Lyapunov exponents⁴⁷.

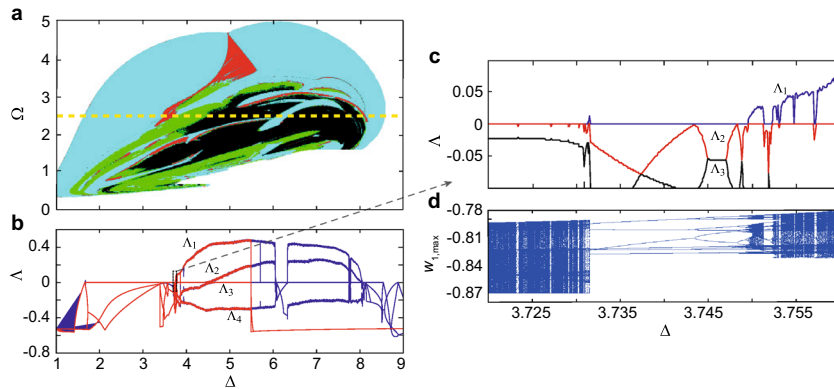


Fig. 2 Hyperchaos in a ring of five qubits. **a** Map showing areas of (Δ, Ω) space corresponding to different regimes of long-term behavior for a ring of five qubits. Black denotes areas of hyperchaos with two positive Lyapunov exponents, green is a region of chaos with one positive Lyapunov exponent, cyan is a periodic regime, red areas correspond to quasiperiodic behavior, and white is a steady-state regime. **b** Variation of the four largest Lyapunov exponents with Δ ; blue dots correspond to Δ increasing from 1 to 9, red dots to Δ decreasing down to 1. **c** A zoom of the region of **b** within the black rectangle. **d** Single-parametric bifurcation diagram corresponding to **c**, in which the vertical positions of each point correspond to the local maxima of $w_1(t)$. For all figures $\Omega = 2.5$.

First we analyze two coupled qubits ($N = 2$). Previously, it has been shown that interplay between the energy pumping and dissipation can eventually trigger self-sustained state population oscillations in this system and even lead to the emergence of bistability, when homogeneous and antiferromagnetic states coexist²⁷. Our investigation reveals another interesting phenomenon associated with deterministic chaos, which emerges via a cascade of period-doubling bifurcations for a periodic oscillations⁴⁷. In Fig. 1c, we show a color map illustrating the dependence of the largest Lyapunov exponent Λ_1 on Δ and Ω . A transition from yellow to black reflects the change from smaller to larger values of Λ_1 . The diagram clearly demonstrates the presence of chaotic dynamics, for which $\Lambda_1 > 0$, in considerable areas of the parameter plane shaded by black color. This shows that the discovered chaos is a robust phenomenon existing in our system over wide parameter ranges. Notably, for certain parameter values it coexists with the antiferromagnetic steady state. The detailed descriptions of the bifurcation transitions and analysis of the Lyapunov exponents that characterize the stability of long-term dynamics are presented in Section B in Supplementary Information.

For $N = 3$ and 4, the same type of chaotic dynamics exists in the system. However, surprisingly, for $N \geq 5$ a new type of chaotic dynamics appears, whose stability is characterized by more than one positive Lyapunov exponent. This type of chaos is known as *hyperchaos*⁴⁸. A map of different dynamical regimes in the (Δ, Ω) parameter plane is shown in Fig. 2a for $N = 5$ and $c = 5$. This diagram was built by calculating the spectrum of Lyapunov exponents for the various limit sets that exist in the (Δ, Ω) -plane. When all the Lyapunov exponents are negative, there is a stable equilibrium state (white in the diagram). If the largest Lyapunov exponent equals 0, the oscillations are periodic (cyan). If the largest two Lyapunov exponents are both 0, the dynamics are quasiperiodic (red). However, when one or two Lyapunov exponents are positive, there is chaos (green) or hyperchaos (black), respectively.

Figure 2b illustrates the bifurcation transitions between the different dynamical regimes when $\Omega = 2.5$ and Δ changes along the yellow dashed line in Fig. 2a. The blue curves represent the evolution of the four largest Lyapunov exponents $\Lambda_1 > \Lambda_2 > \Lambda_3 > \Lambda_4$. A number of distinctive phases emerge as we increase Δ from 1 to 9. The stable equilibrium state, which exists for small Δ , switches to a periodic solution as a result of an Andronov–Hopf bifurcation at $\Delta \approx 1.7$, where Λ_1 becomes zero. At $\Delta \approx 3.55$, the periodic oscillations lose their stability via a Neimark–Sacker

bifurcation, resulting in the onset of quasiperiodic oscillations ($\Lambda_1 = \Lambda_2 = 0$). Increasing Δ further leads to chaotic dynamics.

To better illustrate the transition to the chaotic regime, in Fig. 2c we present a zoom of the region of Fig. 2b framed by the black rectangle. The corresponding bifurcation diagram, shown in Fig. 2d, is constructed by plotting the points corresponding to the local maxima $w_{1,\max}$ in the time evolution of $w_1(t)$, calculated for given Δ . For a particular value of Δ , periodic solutions are represented by one or few single dots on the graph, while the complex sets of many points for a specific Δ reflect quasiperiodic or chaotic dynamics. As Δ increases, the quasiperiodic oscillations where $\Lambda_1 = \Lambda_2 = 0$ (Fig. 2c) are replaced (at $\Delta \approx 3.732$) by complex periodic oscillations due to saddle–node bifurcation. These periodic oscillations are characterized by $\Lambda_1 = 0$ and $\Lambda_{2,3} < 0$ (Fig. 2c) and represented in Fig. 2d by few isolated dots for a fixed Δ . For $\Delta \gtrsim 3.744$, the periodic solutions undergo a cascade of period-doubling bifurcations giving rise to chaos with one positive Lyapunov exponent at $\Delta \approx 3.75$ (Fig. 2c). The period-doubling bifurcations do not affect the spectrum of Lyapunov exponents of the stable solution, since the latter remains periodic. However, each period-doubling causes additional Lyapunov exponent to approach zero (Fig. 2c), which manifests itself via doubling of the number of dots in Fig. 2d. Thus, for $N = 5$, the bifurcation mechanism leading to the onset of chaos stays the same as for the case of $N = 2$. Further investigation shows that this mechanism is also present at larger N .

Increasing Δ makes the chaotic oscillations more complicated and leads to the gradual development of hyperchaos, which emerges at $\Delta \approx 4.4$ (see Fig. 2b). This transition is linked to further instability of already unstable periodic orbits, which form the skeleton of the chaotic attractor. Accumulation of the corresponding bifurcations causes the second Lyapunov exponent to become positive.

We find that period-doubling is the most common but not the only route to chaos exhibited by the system. Figure 2a reveals some direct transitions from the red region where the dynamics is quasiperiodic to the green region where the dynamics are chaotic. This behavior can indicate the mechanism of torus destruction for the transition to chaos^{47,49}. However, we did not specifically investigate the effect of this particular mechanism on the development of hyperchaos.

The dynamics of $N = 5$ coupled qubits in different dynamical regimes is exemplified in Fig. 3. Typical periodic solution is presented in Fig. 3a. Here $n = 1, \dots, 5$ denotes the qubit number in the chain, t is time, and the color scale indicates the value of w_n . All qubits oscillate with the same frequency but with different

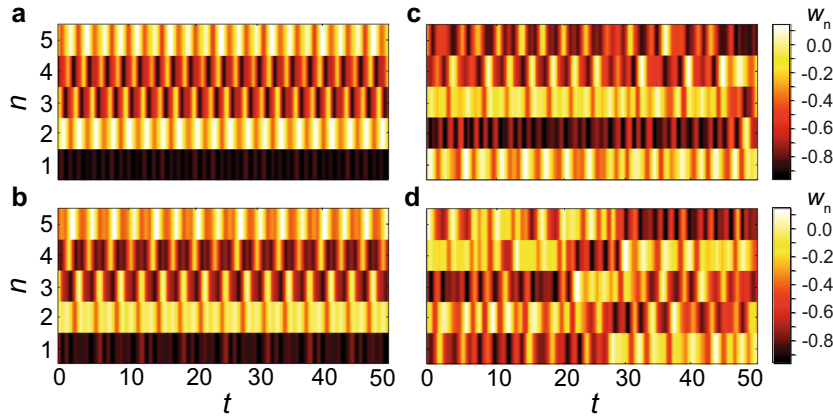


Fig. 3 Time evolution of w_n for 5 qubits. **a** Periodic [$\Delta = 3.74$], **b** quasiperiodic [$\Delta = 3.73$], **c** chaotic [$\Delta = 4.05$], and **d** hyperchaotic [$\Delta = 4.95$] oscillations; n labels an qubit in the chain.

phases. However, the phase shift is constant for each pair of qubits, meaning that they are synchronized. The latter is also indicated by the clearly periodic pattern in Fig. 3a. The quasiperiodic regime when $\Delta = 3.73$ is shown in Fig. 3b. Now the phase shifts between oscillations of different qubits are no longer constant, and the periodic pattern of the spatio-temporal dynamics is lost, reflecting the loss of synchronization.

Chaotic oscillations for $\Delta = 4.05$ are illustrated in Fig. 3c. Here the qubit chain demonstrates erratic behavior, which is in marked contrast to the ordered dynamics presented in Fig. 3a, b. Figure 3d shows typical hyperchaotic oscillations calculated for $\Delta \approx 4.95$. In this regime, the oscillations in the chain become even more complicated than the chaotic behavior in Fig. 3c and now demonstrate no specific time scales in $w_n(t)$. The hyperchaotic behavior persists up to $\Delta \approx 8.0$, after which it rapidly switches to chaotic and then periodic solutions. For $\Delta > 8.53$, all oscillations disappear, and all long-term solutions in the system correspond to stable equilibrium.

In order to further examine the presence of the multistability in the dynamics of the chain, we return to the evolution of the Lyapunov exponents as Δ changes from 9 down to 1. Values of $\Lambda_{1,2,3,4}$ for this case are shown red in Fig. 2b. The plot shows that the stable homogeneous steady state ($\Lambda_1 = \Lambda_2 = \Lambda_3 = \Lambda_4 < 0$) exists down to $\Delta \approx 5.491$, where it suddenly changes to hyperchaotic oscillations. Thus, within the interval of Δ between 5.491 and 9.0, the homogeneous fixed point co-exists with different inhomogeneous regimes, including other types of equilibria, periodic and quasiperiodic oscillations, chaos, and hyperchaos (blue graphs in Fig. 2b). Multistability therefore appears to be a generic phenomenon, existing in chains of different size.

Analysis of chains with $N > 5$ reveals that hyperchaos is not only preserved in the system but also becomes more complicated as more Lyapunov exponents become positive. The results of our analysis are summarized in Fig. 4, where the number of positive Lyapunov exponents, M , is shown as a function of the number of qubits in the chain. The graph shows an almost linear growth, at a rate suggesting that adding two or three qubits leads to the appearance of an additional positive Lyapunov exponent. This phenomenon originates from a weak correlation between the oscillations in distant qubits. As a result, the addition of a subsystem, comprising two or more qubits, is able to demonstrate chaotic dynamics and adds one more positive value to the spectrum of the Lyapunov exponents. Since, for a given coupling, the smallest chaotic subsystem comprises two qubits, their inclusion produces one more positive Lyapunov exponent. The number of Lyapunov exponents grows roughly proportionally to the number N of qubits rather than with the dimensionality 2^N of

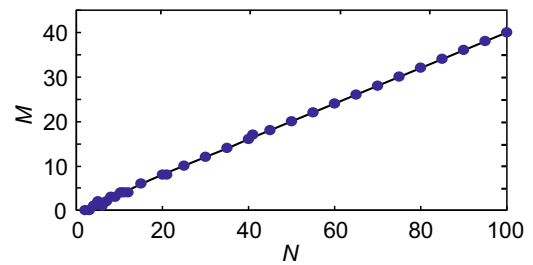


Fig. 4 Number of positive Lyapunov exponents M vs. number of qubits N in the ring chain. $\Delta = 5$, $\Omega = 2.5$, $c = 5$.

the Hilbert space of the system. This indicates the possibility of a reduced description of its dynamics. In such a case, the transitions between qualitatively different, distinct dynamical regimes are controlled by a relatively small number of independent dimensionless parameters.

For large N , multiple positive Lyapunov exponents make the oscillations very complicated, demonstrating broadband continuous spectra, which are similar to random fluctuations in solids⁵⁰. In addition, we found out that these hyperchaotic phenomena are preserved for non-identical qubits and open chains, as well as in chains with more complex qubit-coupling topology than those discussed above. The spatial correlations, the spectra of the chain oscillations calculated for different numbers of qubits, and Lyapunov analysis of chains with non-identical qubits and more complex topology are discussed in Sections C and D in Supplementary Information.

To study the significance of the system's dimensionality, we analyze two-dimensional $L \times L$ lattices of L^2 interacting qubits (Fig. 5a). As for 1D rings, these square lattices exhibit chaotic (for 2×2 lattices) and hyperchaotic behavior (for 3×3 and larger lattices). Figure 5c illustrates the Lyapunov exponents spectrum for a 3×3 square lattice. We observe two areas ($2.7 < \Delta < 3.8$ and $\Delta \approx 5.8$) of chaos, one small area of hyperchaos with two positive Lyapunov exponents ($\Delta \approx 4.2$), and two areas of hyperchaos with three positive exponents ($4.4 < \Delta < 5.3$ and $6.05 < \Delta < 7.6$). Therefore, for a lattice of 9 qubits, we observe a complicated behavior with three positive Lyapunov exponents, which is similar behavior to that we observe for a ring of 9 qubits. We investigate lattices with several values of L of nodes and find almost linear growth of the number of positive Lyapunov exponents with increasing the number of qubits in the lattice (see Fig. 5b). We can conclude that emergence of hyperchaos does not depend on the dimensionality of the system.

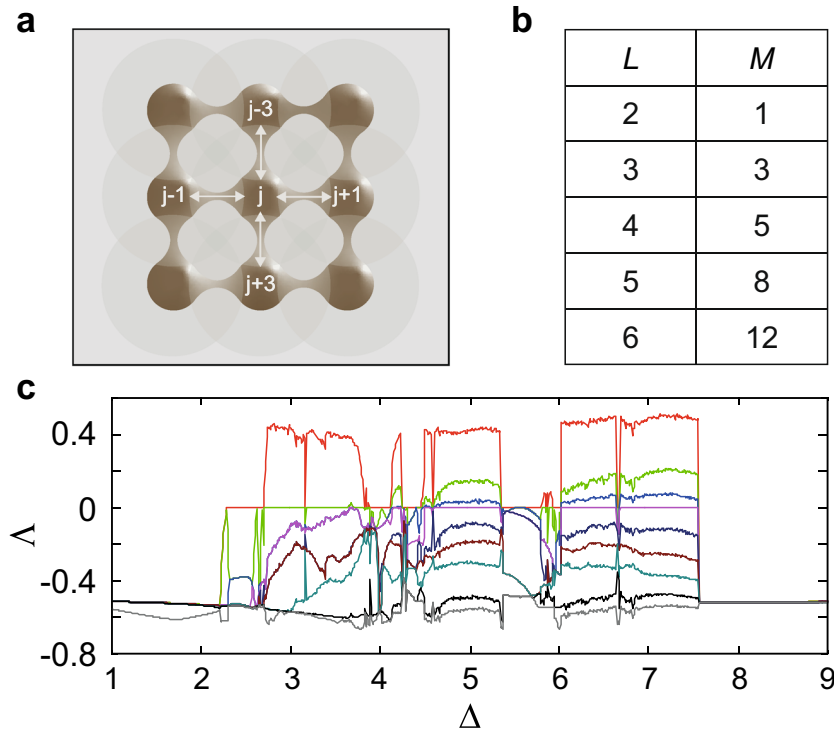


Fig. 5 **2D $L \times L$ lattices of L^2 interacting qubits.** **a** Schematic representation of a square lattice of nine interacting quantum units (e.g., Rydberg atoms or qubits), labeled by integer indexes and coupled via nearest neighbor interactions. **b** Number of positive Lyapunov exponents M vs. lattice size L in the $L \times L$ lattice calculated for $\Delta = 5$, $\Omega = 2.0$, $c = 5$. **c** Variation of the eight largest Lyapunov exponents with Δ for a square lattice of 9 qubits, $\Omega = 2.0$.

Chaos control via a coherent driving field

This dynamical complexity has a deterministic origin, which could be controlled (suppressed or enhanced) by an applied external field. Previously, it was demonstrated that a periodic perturbation can suppress hyperchaos with two positive Lyapunov exponents^{51,52}. Here we apply a periodic modulation to the laser field amplitude, which modulates the Rabi frequency:

$$\Omega = \Omega_m [1 + M \sin(2\pi f t)], \quad (5)$$

where Ω_m is the amplitude of the Rabi frequency, while M and f are the modulation index and the frequency of modulation, respectively. We consider the case when $N = 15$, a large but practically feasible number of qubits such that the system shows hyperchaos, characterized by four positive Lyapunov exponents and a broadband spectrum. Figure 6 presents the 11 largest conditional Lyapunov exponents (Fig. 6a) and the corresponding bifurcation diagram (Fig. 6b) calculated for $\Omega_m = 2.5$, $c = 5$, $\Delta = 5.0$, $M = 0.684$, and f changing from 0 to 2.0.

Due to the periodic modulation, chaos is suppressed in certain parameter regions. For f between 0.7 and 0.8, we find complex periodic oscillations characterized by the largest Lyapunov exponent < 0 (see Fig. 6a) and multiple branches in the bifurcation diagram (Fig. 6b). Within the interval $f \in (0.9, 1.1)$, we find periodic oscillations (one maxima per period) and Lyapunov exponents $\ll 0$, corresponding to highly stable regular oscillations in this regime. In addition, the same controlling signal is able to significantly increase the complexity of hyperchaotic oscillations and a corresponding increase in the value of the largest Lyapunov exponent. For example, when $f \approx 0.3$ the largest Lyapunov exponent becomes almost three times larger than in the case without the application of the signal ($f = 0$). Otherwise the number of positive Lyapunov exponents can be increased by 1 ($f = 1.2$) or 2 ($f = 1.4$). Our results demonstrate that periodic modulation of laser field amplitude can be used as an efficient method to control very complex hyperchaos in qubit arrays.

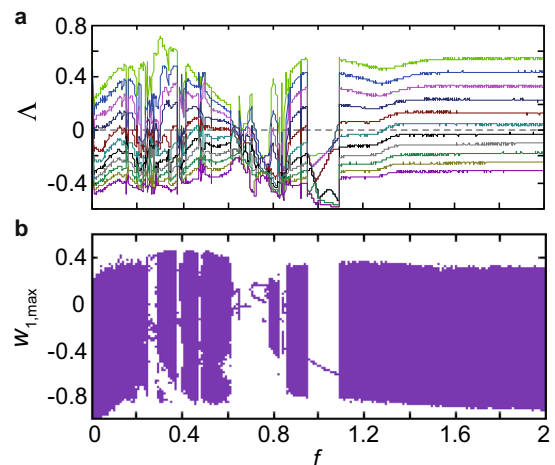


Fig. 6 **Chaos control.** **a** Conditional Lyapunov exponents spectrum and **b** bifurcation diagram for a ring of 15 qubits by means of an external parametric effect for $\Omega_m = 2.5$, $c = 5$, $\Delta = 5.0$, $M = 0.684$.

DISCUSSION

We have shown that the interplay between dissipation and energy pumping in quantum systems comprising chains of qubits can produce highly nontrivial emergent phenomena associated with the onset of complex chaotic and hyperchaotic oscillations even in the absence of multi-particle entanglement. The complexity of the hyperchaos increases with the number of elements in the chain. The number of positive Lyapunov exponents grows linearly with the number of qubits, that is, as only log of the dimensionality of the Hilbert space. This indicates the possibility of a reduced description of the quantum system by a small (in comparison to the dimensionality of the Hilbert space) number of dimensionless

parameters. This observation is consistent with the fact that the manifold of all quantum states that can be generated by arbitrary time-dependent local Hamiltonians in a polynomial time occupies an exponentially small volume in the Hilbert space of the system⁵³.

Our results demonstrate a mechanism for randomizing the evolution of coupled qubits, which arises due to dynamical phenomena far from equilibrium and is thus unrelated to thermalization processes despite the superficial similarity. The model we have used is generic and can be applied and implemented directly in, e.g., chains of qubits or electromagnetically driven superconducting qubits. Our results will be important for the development of large quantum systems, where multi-point entanglement is neither required nor supported^{42,43,54}. In particular, they suggest a controllable way of switching between different dynamical regimes via regular to chaos transitions either by tuning the parameters of the system or by applying a controlling signal via modulation of laser field amplitude, as another approach towards controlling quantum state dynamics⁵⁵. Our results are of interest for the development of quantum random number generators⁵⁶ and quantum chaotic cryptography^{57,58}. A natural extension of this research will consider the effect of interqubit entanglement on the complexity revealed here and whether it can be utilized for controlling this far-from-equilibrium behavior.

Another interesting task will be to study how quantum signatures of classical chaos such as the growth rate of out-of-time-ordered correlators⁵⁹ behave in the presence of hyperchaos. Preliminary results on the integration of the original quantum model (Eq. (2)), briefly discussed in Section E in Supplementary Information, indicate that the complexity of chain dynamics depends highly non-trivially on the parameters of the Hamiltonian (Eq. (1)). However, a detailed analysis of the dynamical regimes and their characteristics in the presence of entanglement, and especially of the question about the universality of these regimes and parameters that control them, requires extensive further research, which we hope this paper will stimulate.

METHODS

Lyapunov exponents calculation

The Lyapunov exponents were calculated for the stable limit sets, which correspond to the solutions of the model equations as time $t \rightarrow \infty$. Since we apply the periodic modulation (Eq. (5)) to the system (Eq. (4)), the Lyapunov exponents we calculate in this case are called conditional and missing one zero exponent, unlike the common Lyapunov exponents spectrum⁶⁰. To determine them, we implement $3N$ perturbations vectors, where N is the number of units in the system, and use periodic Gram–Schmidt orthonormalization of the Lyapunov vectors to avoid a misalignment of all the vectors along the direction of maximal expansion^{61,62}.

Bifurcation diagrams

In order to construct a bifurcation diagram, we plot the points corresponding to the local maxima $w_{1,\max}$ in the time evolution of $w_1(t)$, calculated for given Δ and Ω .

DATA AVAILABILITY

The data that support the findings of this study are available from the corresponding authors upon reasonable request.

CODE AVAILABILITY

All codes used in the paper are available from the corresponding authors upon reasonable request.

Received: 14 May 2020; Accepted: 4 November 2020;

Published online: 04 January 2021

REFERENCES

- Walport, M. & Knight, P. *The Quantum Age: Technological Opportunities* (Government Office for Science, 2016).
- Georgescu, I. & Nori, F. Quantum technologies: an old new story. *Phys. World* **25**, 16 (2012).
- Knight, P. & Walmsley, I. UK national quantum technology programme. *Quantum Sci. Technol.* **4**, 040502 (2019).
- Acín, A. et al. The quantum technologies roadmap: a European community view. *N. J. Phys.* **20**, 080201 (2018).
- Zurek, W. H. Decoherence, einselection, and the quantum origins of the classical. *Rev. Mod. Phys.* **75**, 715 (2003).
- Zurek, W. H. Quantum Darwinism. *Nat. Phys.* **5**, 181–188 (2009).
- Xiong, H.-N., Lo, P.-Y., Zhang, W.-M., Feng, D. H. & Nori, F. Non-Markovian complexity in the quantum-to-classical transition. *Sci. Rep.* **5**, 13353 (2015).
- Lambert, N., Chen, Y.-n, Johansson, R. & Nori, F. Quantum chaos and critical behavior on a chip. *Phys. Rev. B* **80**, 165308 (2009).
- Aßmann, M., Thewes, J., Fröhlich, D. & Bayer, M. Quantum chaos and breaking of all anti-unitary symmetries in Rydberg excitons. *Nat. Mater.* **15**, 741–745 (2016).
- Fiderer, L. J. & Braun, D. Quantum metrology with quantum-chaotic sensors. *Nat. Commun.* **9**, 1–9 (2018).
- Gao, T. et al. Observation of non-Hermitian degeneracies in a chaotic exciton-polariton billiard. *Nature* **526**, 554–558 (2015).
- Zhu, G.-L. et al. Single-photon-triggered quantum chaos. *Phys. Rev. A* **100**, 023825 (2019).
- Chaudhury, S., Smith, A., Anderson, B., Ghose, S. & Jessen, P. S. Quantum signatures of chaos in a kicked top. *Nature* **461**, 768–771 (2009).
- Zhang, W., Sun, C. & Nori, F. Equivalence condition for the canonical and micro-canonical ensembles in coupled spin systems. *Phys. Rev. E* **82**, 041127 (2010).
- Neill, C. et al. Ergodic dynamics and thermalization in an isolated quantum system. *Nat. Phys.* **12**, 1037–1041 (2016).
- Turner, C. J., Michailidis, A. A., Abanin, D. A., Serbyn, M. & Papić, Z. Weak ergodicity breaking from quantum many-body scars. *Nat. Phys.* **14**, 745–749 (2018).
- Lewis-Swan, R., Safavi-Naini, A., Bollinger, J. J. & Rey, A. M. Unifying scrambling, thermalization and entanglement through measurement of fidelity out-of-time-order correlators in the dicke model. *Nat. Commun.* **10**, 1–9 (2019).
- Dowling, J. P. & Milburn, G. J. Quantum technology: the second quantum revolution. *Philos. Trans. R. Soc. Lond. Ser. A Math. Phys. Eng. Sci.* **361**, 1655–1674 (2003).
- Hegel, G. W. F. *The Science of Logic* (Cambridge University Press, 2015).
- Engels, F. *Anti-Dühring Herr Eugen Dühring's Revolution in Science* (Progress, 1969).
- Piazza, F. & Ritsch, H. Self-ordered limit cycles, chaos, and phase slippage with a superfluid inside an optical resonator. *Phys. Rev. Lett.* **115**, 163601 (2015).
- Zhang, M., Shah, S., Cardenas, J. & Lipson, M. Synchronization and phase noise reduction in micromechanical oscillator arrays coupled through light. *Phys. Rev. Lett.* **115**, 163902 (2015).
- Ozyuzer, L. et al. Emission of coherent THz radiation from superconductors. *Science* **318**, 1291–1293 (2007).
- Savel'ev, S., Yampol'skii, V., Rakhmanov, A. & Nori, F. Terahertz Josephson plasma waves in layered superconductors: spectrum, generation, nonlinear and quantum phenomena. *Rep. Prog. Phys.* **73**, 026501 (2010).
- Welp, U., Kadowaki, K. & Kleiner, R. Superconducting emitters of THz radiation. *Nat. Photonics* **7**, 702–710 (2013).
- Weimer, H., Müller, M., Lesanovsky, I., Zoller, P. & Büchler, H. P. A Rydberg quantum simulator. *Nat. Phys.* **6**, 382–388 (2010).
- Lee, T. E., Häffner, H. & Cross, M. Antiferromagnetic phase transition in a nonequilibrium lattice of Rydberg atoms. *Phys. Rev. A* **84**, 031402 (2011).
- Lee, T. E., Häffner, H. & Cross, M. Collective quantum jumps of Rydberg atoms. *Phys. Rev. Lett.* **108**, 023602 (2012).
- Ostrovskaya, E. A. & Nori, F. Giant Rydberg excitons: probing quantum chaos. *Nat. Mater.* **15**, 702–703 (2016).
- Labuhn, H. et al. Tunable two-dimensional arrays of single Rydberg atoms for realizing quantum Ising models. *Nature* **534**, 667–670 (2016).
- Minganti, F., Miranowicz, A., Chhajlany, R. W. & Nori, F. Quantum exceptional points of non-Hermitian Hamiltonians and Liouvillians: the effects of quantum jumps. *Phys. Rev. A* **100**, 062131 (2019).
- Bendkowsky, V. et al. Observation of ultralong-range Rydberg molecules. *Nature* **458**, 1005–1008 (2009).
- Löw, R. Rydberg atoms: two to tango. *Nat. Phys.* **10**, 901–902 (2014).
- Basak, S., Chougale, Y. & Nath, R. Periodically driven array of single Rydberg atoms. *Phys. Rev. Lett.* **120**, 123204 (2018).

35. Butscher, B. et al. Atom–molecule coherence for ultralong-range Rydberg dimers. *Nat. Phys.* **6**, 970–974 (2010).
36. Niederprüm, T. et al. Observation of pendular butterfly Rydberg molecules. *Nat. Commun.* **7**, 1–6 (2016).
37. Eiles, M. T., Tong, Z. & Greene, C. H. Theoretical prediction of the creation and observation of a ghost trilobite chemical bond. *Phys. Rev. Lett.* **121**, 113203 (2018).
38. Zeiher, J. et al. Coherent many-body spin dynamics in a long-range interacting Ising chain. *Phys. Rev. X* **7**, 041063 (2017).
39. Labuhn, H. et al. Tunable two-dimensional arrays of single Rydberg atoms for realizing quantum Ising models. *Nature* **534**, 667–670 (2016).
40. Barredo, D. et al. Coherent excitation transfer in a spin chain of three Rydberg atoms. *Phys. Rev. Lett.* **114**, 113002 (2015).
41. Saffman, M., Walker, T. G. & Mølmer, K. Quantum information with Rydberg atoms. *Rev. Mod. Phys.* **82**, 2313 (2010).
42. Zagoskin, A., Rakhmanov, A., Savel'ev, S. & Nori, F. Quantum metamaterials: electromagnetic waves in Josephson qubit lines. *Phys. Status Solidi B* **246**, 955–960 (2009).
43. Macha, P. et al. Implementation of a quantum metamaterial using superconducting qubits. *Nat. Commun.* **5**, 1–6 (2014).
44. Gaul, C. et al. Resonant Rydberg dressing of alkaline-earth atoms via electromagnetically induced transparency. *Phys. Rev. Lett.* **116**, 243001 (2016).
45. Zeiher, J. et al. Many-body interferometry of a Rydberg-dressed spin lattice. *Nat. Phys.* **12**, 1095–1099 (2016).
46. Aolita, L., De Melo, F. & Davidovich, L. Open-system dynamics of entanglement: a key issues review. *Rep. Prog. Phys.* **78**, 042001 (2015).
47. Anishchenko, V. S. *Dynamical Chaos, Models and Experiments: Appearance Routes and Structure of Chaos in Simple Dynamical Systems* (World Scientific Publishing, Singapore, 1995).
48. Rossler, O. An equation for hyperchaos. *Phys. Lett. A* **71**, 155–157 (1979).
49. Field, S., Venturi, N. & Nori, F. Marginal stability and chaos in coupled faults modeled by nonlinear circuits. *Phys. Rev. Lett.* **74**, 74 (1995).
50. Kogan, S. *Electronic Noise and Fluctuations in Solids* (Cambridge University Press, 2008).
51. Xiao-Hui, Z. & Ke, S. The control action of the periodic perturbation on a hyperchaotic system. *Acta Phys. Sin. (Overseas Ed.)* **8**, 651 (1999).
52. Sun, K., Liu, X., Zhu, C. & Sprott, J. Hyperchaos and hyperchaos control of the sinusoidally forced simplified Lorenz system. *Nonlinear Dynamics* **69**, 1383–1391 (2012).
53. Poulin, D., Qarry, A., Somma, R. & Verstraete, F. Quantum simulation of time-dependent Hamiltonians and the convenient illusion of Hilbert space. *Phys. Rev. Lett.* **106**, 170501 (2011).
54. Fitzpatrick, M., Sundaresan, N. M., Li, A. C., Koch, J. & Houck, A. A. Observation of a dissipative phase transition in a one-dimensional circuit QED lattice. *Phys. Rev. X* **7**, 011016 (2017).
55. Zhang, J., Liu, Y.-x., Wu, R.-B., Jacobs, K. & Nori, F. Quantum feedback: theory, experiments, and applications. *Phys. Rep.* **679**, 1–60 (2017).
56. Herrero-Collantes, M. & Garcia-Escartin, J. C. Quantum random number generators. *Rev. Mod. Phys.* **89**, 015004 (2017).
57. Monifi, F. et al. Optomechanically induced stochastic resonance and chaos transfer between optical fields. *Nat. Photonics* **10**, 399–405 (2016).
58. de Oliveira, G. & Ramos, R. V. Quantum-chaotic cryptography. *Quantum Inf. Process.* **17**, 40 (2018).
59. Chávez-Carlos, J. et al. Quantum and classical Lyapunov exponents in atom-field interaction systems. *Phys. Rev. Lett.* **122**, 024101 (2019).
60. Pyragas, K. Conditional Lyapunov exponents from time series. *Phys. Rev. E* **56**, 5183 (1997).
61. Oseledets, V. I. A multiplicative ergodic theorem. Characteristic Lyapunov exponents of dynamical systems. *Trans. Moscow Math. Soc.* **19**, 197–231 (1968).
62. Wolf, A., Swift, J. B., Swinney, H. L. & Vastano, J. A. Determining Lyapunov exponents from a time series. *Phys. D Nonlinear Phenom.* **16**, 285–317 (1985).

ACKNOWLEDGEMENTS

A.M.Z. and A.G.B. thank Professor S. Watabe for illuminating discussions. This work was supported in part by EPSRC (grant EP/M006581/1), the grant from the Ministry of Science and Higher Education of the Russian Federation in the framework of Increase Competitiveness Program of NUST MISIS, Grant No. K2-2020-001, and Russian Foundation for Basic Research (RFBR) 18-32-20135. W.L. acknowledges support from the UKIERI-UGC Thematic Partnership No. IND/CONT/G/16-17/73, EPSRC Grant No. EP/R04340X/1, and support from the University of Nottingham.

AUTHOR CONTRIBUTIONS

A.M.Z., A.G.B., and A.E.H. conceived, designed, and supervised the project. The theoretical calculations were performed by A.M.Z. (analytical) and A.V.A., V.V.M., A.E.H. and A.G.B. (numerical). A.G.B., A.E.H., T.M.F., M.T.G., W.L., and A.M.Z. analyzed the data and wrote the manuscript. All authors discussed the results and contributed to the manuscript.

COMPETING INTERESTS

The authors declare no competing interests.

ADDITIONAL INFORMATION

Supplementary information is available for this paper at <https://doi.org/10.1038/s41534-020-00339-1>.

Correspondence and requests for materials should be addressed to A.G.B. or A.M.Z.

Reprints and permission information is available at <http://www.nature.com/reprints>

Publisher's note Springer Nature remains neutral with regard to jurisdictional claims in published maps and institutional affiliations.



Open Access This article is licensed under a Creative Commons Attribution 4.0 International License, which permits use, sharing, adaptation, distribution and reproduction in any medium or format, as long as you give appropriate credit to the original author(s) and the source, provide a link to the Creative Commons license, and indicate if changes were made. The images or other third party material in this article are included in the article's Creative Commons license, unless indicated otherwise in a credit line to the material. If material is not included in the article's Creative Commons license and your intended use is not permitted by statutory regulation or exceeds the permitted use, you will need to obtain permission directly from the copyright holder. To view a copy of this license, visit <http://creativecommons.org/licenses/by/4.0/>.

© The Author(s) 2021